

Corrosion and Cavitation Erosion Behaviors of Friction Stir Processed Ni-Al Bronze: Effect of Processing Parameters and Position in the Stirred Zone

Q.N. Song,* Y.G. Zheng,^{†*} D.R. Ni,** and Z.Y. Ma**

ABSTRACT

As-cast Ni-Al bronze (NAB) was subjected to friction stir processing (FSP). Different processing parameters including rotating rate, traverse speed, and processing passes were selected to investigate their effect on the corrosion and cavitation erosion properties. Polarization curve and electrochemical impedance spectroscopy (EIS) were used to reveal the corrosion behavior. Cavitation erosion tests were conducted with an ultrasonic vibration device, and the eroded surfaces were observed using scanning electron microscopy (SEM). Results showed that cavitation erosion resistance was improved for all the processed NAB compared to the as-cast, and a two-pass processed NAB possessed the best corrosion resistance since it had further homogenized microstructure compared to the single-pass processed ones. Corrosion and cavitation erosion tests were also conducted on samples (Surface, Subsurface, Middle, and Bottom) obtained by machining from different positions of the stirred zone (SZ) in a constant-parameter processed NAB along the plate thickness. The Middle was more corrosion resistant since its equiaxed microstructure contributed to a homogeneous oxide film on the surface. The grains in the Bottom were the finest, so the Bottom was the most cavitation erosion resistant.

KEY WORDS: cavitation erosion, corrosion, friction stir processing, Ni-Al bronze

INTRODUCTION

Friction stir processing (FSP) is a solid-state processing method that is operated below the melting point of the materials. A rotating tool, which is not consumable, inserts into a component and then traverses along the desired path to modify the microstructure.¹ This method is based on friction stir welding (FSW) developed in 1991.² FSP, a different form of FSW, is used to modify the surface of a single component and no joint is created. FSP has been used in the castings since it can transform the cast microstructure to a wrought-like state through severe plastic deformation, and eliminate casting porosities.³ The mechanical properties, erosion, and corrosion resistance were reported to be greatly improved after FSP for aluminum-,⁴⁻⁵ copper-,⁶⁻⁸ titanium-,⁹ magnesium-,¹⁰⁻¹¹ and iron-based¹²⁻¹³ alloys, etc. Research has also suggested that the processing parameters of FSP, including the traversing speed and rotating rate of the tool, tool design, and over-lapping of the multiple passes, greatly influenced the above properties.¹⁴⁻¹⁶ The stirred zone (SZ) of the processed Ni-Al bronze (NAB) plate was characterized by heterogeneous microstructure at different depths from the plate surface by Ni, Oh-ishi, and coworkers.^{6,8} Xu, et al., investigated the microstructure and pitting corrosion behavior along the depth of the welded nugget zone in the friction stir welded 2219-O (UNS A92219)⁽¹⁾ aluminum alloy; it was reported that the size of second-phase particles

Submitted for publication: June 29, 2013. Revised and accepted: September 19, 2013. Preprint available online: October 1, 2013. doi: <http://dx.doi.org/10.5006/1070>.

[†] Corresponding author. E-mail: ygzhen@imr.ac.cn.

* State Key Laboratory for Corrosion and Protection, Institute of Metal Research, Chinese Academy of Sciences, 62 Wencui Road, Shenyang 110016, China.

** Shenyang National Laboratory for Materials Science, Institute of Metal Research, Chinese Academy of Sciences, 72 Wenhua Road, Shenyang 110016, China.

⁽¹⁾ UNS numbers are listed in *Metals and Alloys in the Unified Numbering System*, published by the Society of Automotive Engineers (SAE International) and cosponsored by ASTM International.

TABLE 1
Friction Stir Processing Parameters

Processing parameters	1200/50	1200/100	1200/50-double	1500/50
Rotating rate (rpm)	1,200	1,200	1,200	1,500
Traversing speed (mm/min)	50	100	50	50
Processing passes	1	1	2 ^(A)	1

^(A) 100% over-lapping between the two passes.

Al₂Cu increased from the top to the Bottom of the weld nugget zone, and the top had the highest pitting corrosion resistance.¹⁷

NAB is widely used in marine environments because of its high corrosion and cavitation erosion resistance.¹⁸⁻¹⁹ It is one of the main materials for ship propellers. Since the propeller rotates at high speed in seawater, it suffers both corrosion and cavitation erosion. Cavitation erosion is a common mode of material degradation in marine systems. The fluctuation of pressure in liquids results in the generation and collapse of bubbles. Adjacent liquid with the collapsing energy of the bubbles impacts on the components as a micro-jet or shock wave and causes deformation and mass loss.²⁰ Many studies showed that higher mechanical properties, such as ultimate resilience and fatigue strength, contributed to higher cavitation erosion resistance of the alloys.²¹⁻²² Propellers are always cast in large sizes, and the as-cast NAB mainly contains coarse Widmanstätten α phase, Fe- or Ni-rich κ phases, and martensite β' phase.²³⁻²⁴ The coarse and inhomogeneous cast microstructure, as well as the inevitable casting defects, is detrimental to the life of the propeller. Many methods have been explored to compensate for these, such as producing coatings on the surface of the substrate through surface laser melting and alloying,²⁵⁻²⁶ friction surfacing,²⁷ and HVOF (high velocity oxygen fuel) thermal spray.²⁸ Besides these, FSP is another novel surface processing method.

FSP was primarily applied to repair and locally enhance the NAB propellers by the U.S. Naval Surface Warfare Center, Carderock Division (West Bethesda, Maryland).²⁹ Subsequent research also investigated the microstructure and mechanical properties of as-cast NAB after FSP in detail.^{6,8,14} Furthermore, recently in our studies, the corrosion and cavitation erosion behaviors of the as-cast and friction stir processed NAB were studied.³⁰ Ni, Oh-ishi, and co-workers reported that processing parameters of FSP influenced the microstructure and mechanical properties of NAB. Besides, the microstructure in the SZ was also reported to be heterogeneous.^{6,14} However, the effect of the processing parameters on the corrosion and cavitation erosion behaviors of NAB attracted less attention. Additionally, whether the heterogeneous microstructure could cause the heterogeneity of corrosion and cavitation erosion resistance in the SZ was also not clear.

The present study tried to document how the processing parameters of FSP influenced the corrosion and cavitation erosion resistance of as-cast NAB. The corrosion and cavitation erosion behaviors of samples, which were sectioned from the SZ of a constant-parameter-processed NAB along the plate thickness, were also investigated.

EXPERIMENTAL PROCEDURES

Material and Medium

The material used in this investigation was UNS C95800 NAB (chemical composition in wt%: Al 9.18, Ni 4.49, Fe 4.06, Mn 1.03, and Cu balance). The processing details of FSP were reported previously.⁶ The 300 mm by 70 mm by 8 mm casting NAB plates were subjected to FSP with different processing parameters. In the present study, four combinations of rotating rate, traversing speed, and processing passes were investigated, as listed in Table 1.

Microstructure was observed using a metallographic microscope, after being etched with the solution of 5 g iron(III) chloride (FeCl₃) + 2 mL hydrochloric acid (HCl) + 95 mL ethanol (C₂H₅OH) for the as-cast and the processed NAB with different processing parameters.

For all the processed NAB, samples for the cavitation erosion test (the working surface seen in Figure 1[b]) were sectioned along the processing direction (the sampling location seen in Figure 1[a]), while samples for the corrosion test under quiescence conditions were cut from the center of the SZ in the cross section of the plate, with a 7 mm by 7 mm working area (the sampling location seen in Figure 1[c]) exposed to the medium, which was 3.5 wt% sodium chloride (NaCl) solution made up from analytical grade reagent and distilled water.

1200/50 was selected for the study of cavitation erosion and corrosion behaviors at different positions of the SZ along the plate thickness. The SZ was cut into four pieces according to the positions of four different microstructures in the SZ (details as follows), Figure 1(d). The four pieces were named according to their depth from the surface of the plate as Surface, Subsurface, Middle, and Bottom, respectively. Their thicknesses were about 1.2 mm, 2 mm, 3 mm, and 1.2 mm, respectively (with loss during machining excluded). Sample for the cavitation erosion test was of the same size as that for the corrosion test, namely, with 7 mm by 7 mm as the area of the working surface.

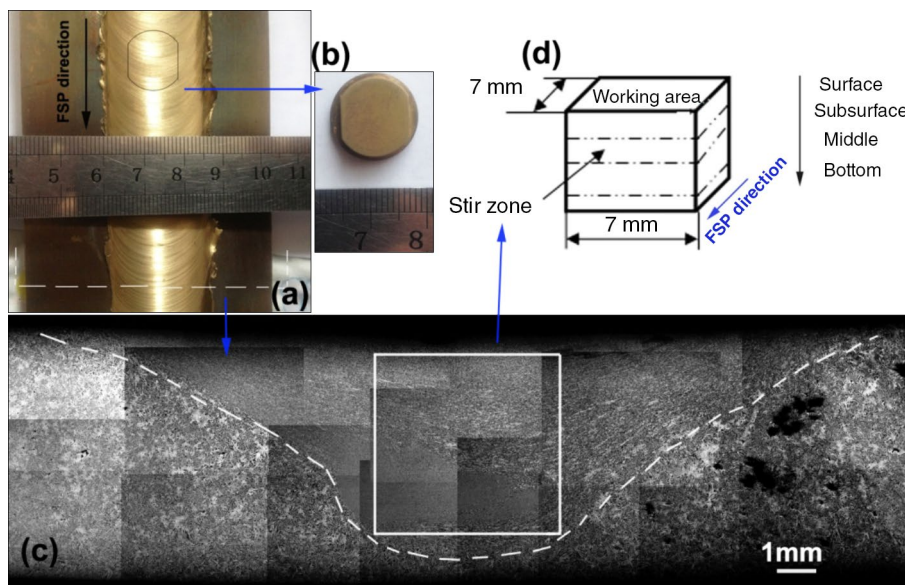


FIGURE 1. (a) Top view of processed NAB, (b) sample after cavitation erosion test, (c) cross-sectional graph of processed NAB, and (d) schematic graphs for sampling at different positions in SZ.

The surface was mechanically ground with abrasive papers and polished to a 1 μm diamond finish for all the samples; all the tests were repeated at least three times to ensure accuracy.

Electrochemical Measurements

The electrochemical tests were operated in a typical three-electrode cell with a platinum foil as the counter electrode and a saturated calomel electrode (SCE) as the reference electrode. Polarization curves were recorded at a sweep rate of 0.333 mV/s from -0.3 V to 1.2 V vs. the open-circuit potential. Electrochemical impedance spectroscopy (EIS) tests were carried out from 100 kHz to 10 mHz under quiescence conditions, and from 20 kHz to 100 mHz under cavitation erosion conditions with a 5 mV perturbation.

Cavitation Erosion Tests

Cavitation erosion tests were carried out according to the ASTM G32 standard.³¹ The frequency and amplitude of the vibrating horn were 20 kHz and 60 μm , respectively. The test sample was held 0.5 mm right below the horn and immersed 15 mm below the surface of the medium, which was kept at about 20°C by cycling cooling water. The sample was ultrasonically cleaned, dried with blowing air, and weighed initially and after cavitation erosion for different times. Scanning electron microscopy (SEM) was used for the surface morphology observation.

RESULTS

Microstructure

As seen in Figure 2, as-cast NAB is composed of lightly etched, coarse Widmanstätten α phase,

which is more than 100 μm , darkly etched β' and κ phases (Figure 2[a]). κ phases contain fine κ_{IV} inside α phase, κ_{II} and lamellar eutectoid κ_{III} mainly at the phase boundaries (Figure 2[b]). The SZ is characterized by four different microstructures along the plate thickness for all of the processed NAB with different parameters, which is Widmanstätten α and fine β' (β transformation product) phases in the Surface (Figure 2[c]), banded α and β' in the Subsurface (Figure 2[d]), equiaxed α and β' in the Middle (Figure 2[e]), and stream-like α and β' in the Bottom (Figure 2[f]). Finer α grains are found inside the banded and stream-like structures, and the stream-like structure contains the finest α with a grain size of 2 μm ~ 3 μm . The proportion of each microstructure in the SZ is different for the processed NAB with different processing parameters. The SZ of 1200/50-double consists mainly of the equiaxed microstructure.

Corrosion and Cavitation Erosion Behaviors of Processed Ni-Al Bronzes with Different Processing Parameters

Figure 3(a) shows Nyquist plots of the NAB samples with different processing parameters. The larger semi-diameter in the Nyquist plots indicates better corrosion resistance.³² 1200/50-double is the most corrosion resistant. Compared with 1200/50, the corrosion resistance decreases slightly by increasing the rotating rate to 1,500 rpm or the traverse speed to 100 mm/min. Polarization curves of the processed NAB are similar, as shown in Figure 3(b). The surface morphologies for 1500/50 and 1200/50-double before and after being polarized are shown in Figure 4. The corroded surface after polarization for 1500/50, as well as 1200/50, 1200/100 (not shown), is very

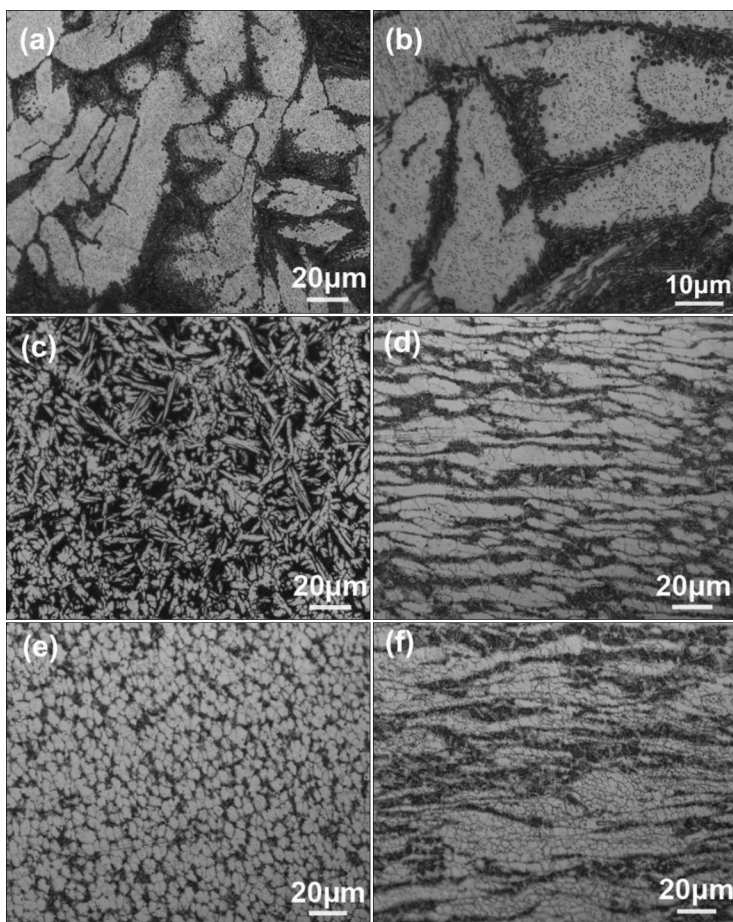


FIGURE 2. Optical micrographs of as-cast NAB and SZ of 1500/50. As-cast NAB: (a) coarse Widmanstätten morphology at lower magnification, (b) multiple phases shown at large magnification; SZ of 1500/50: (c) fine Widmanstätten structure at Surface, (d) banded structure at Subsurface, (e) equiaxed structure at Middle, (f) stream-like structure at Bottom along the plate thickness.

rough and uneven with large pits in some areas. Pits are found mainly at the positions with Widmanstätten, banded, and stream-like microstructures. The position with equiaxed microstructure is evenly corroded, and no large pits are found there, as shown in Figure 4(c). However, for 1200/50-double, the surface after polarization is uniformly corroded in Figure 4(d).

Figure 5 shows the cumulative mass loss of the processed NAB with different processing parameters under cavitation erosion in 3.5 wt% NaCl solution. The results of the as-cast NAB and 1200/50, which were reported already in our previous study, act as references here.³⁰ It is obvious that the cavitation erosion resistance is improved for all of the investigated processing parameters compared with that of the as-cast. However, there is small difference among the processed NAB since the error bars, which are calculated from at least three parallel tests, overlap with each other. In spite of the overlapping results, the order of cavitation erosion resistance is roughly as follows: 1200/50 < 1500/50 < 1200/50-double < 1200/100.

EIS tests under cavitation erosion were also conducted for all the processed NAB samples with different processing parameters to monitor the surface change under cavitation erosion. All of the test results are very similar, so only the results of 1200/100 are presented here. Figure 6 shows that with increasing the cavitation erosion time, the semi-diameter of the capacitive reactance arc in the first quadrant of the Nyquist plot decreases, and there is an inductive arc at the lower frequency in the Nyquist plot.

The damaged surface morphologies for 1200/100 after different cavitation erosion times are presented in Figure 7. After cavitation erosion for 1 h, extrusions are found mainly in the α phase and there are already small cavities on the surface, as seen in Figure 7(a). After cavitation erosion for 3 h, most of the surface suffers damage; larger cavities are all over the surface (Figure 7[b]). After cavitation erosion for 5 h, the original surface no longer exists, cavities grow and join together to form larger ones (Figure 7[c]). For the as-cast NAB, larger cavities already appear after cavitation erosion for 5 h (Figure 7[e]), and honeycombed

cavities widely spread on the whole surface for 16 h (Figure 7[f]). While for 1200/100, the surface after cavitation erosion for 20 h is still relatively smooth, as seen in Figure 7(d).

Corrosion and Cavitation Erosion Behaviors Along the Plate Thickness in the Stirred Zone

Figure 8 shows the electrochemical results of the four different positions. The initial Nyquist plots (Figure 8[a]) and polarization curves (Figure 8[b]) are similar for the four positions. Figure 8(c) shows the EIS results after immersion in 3.5 wt% NaCl solution for different times to monitor the surface change. For all four positions, the electrochemical impedance after 10 days' immersion increases compared to the initial impedance shown in Figure 8(a). Except for the Bottom, the electrochemical impedance increases with the immersion time. Besides, the electrochemical impedance of the Middle is the largest after 10 days' immersion.

Figure 9 shows the cumulative mass loss for the four positions as a function of the cavitation erosion time. The Bottom is the most cavitation-erosion-resistant, followed by the Surface, Middle, and Subsurface.

Figure 10 shows the damaged surface morphologies for the samples at different positions. After cavitation erosion for 1 h, extrusions are clearly seen in α phase, and the detachment of β' phase is exhibited for all the samples. After cavitation erosion for 3 h, the microstructure is clearly recognized and more cavities appear on the surface. Cavities are seen not only at the phase boundaries between α and β' , but also inside α phase for the banded and equiaxed microstructures (Figures 10[f] and [g]). Furthermore, cracks also appear at the grain boundaries of the finer α phase inside the banded and stream-like structures (Figures 10[f] and [h]). In comparison, the stream-like and Widmanstätten structures suffer less damage.

DISCUSSION

The detailed discussion on the microstructures in the SZ of processed NAB with different processing parameters were presented in our previous study;⁶ the main contribution in this study was to explore the difference of corrosion and cavitation erosion behaviors caused by the processing parameters and the microstructure heterogeneity in the SZ.

Effect of Processing Parameters on the Corrosion and Cavitation Erosion Behaviors of Processed Ni-Al Bronzes

Corrosion Behavior — From Figure 3, 1500/50 and 1200/100 exhibited inferior corrosion resistance compared with 1200/50. It could be explained as follows. When the rotating rate increased to 1,500 rpm, the heat input increased, thus promoting the growth of the recrystallized grains. Higher rotating rates also

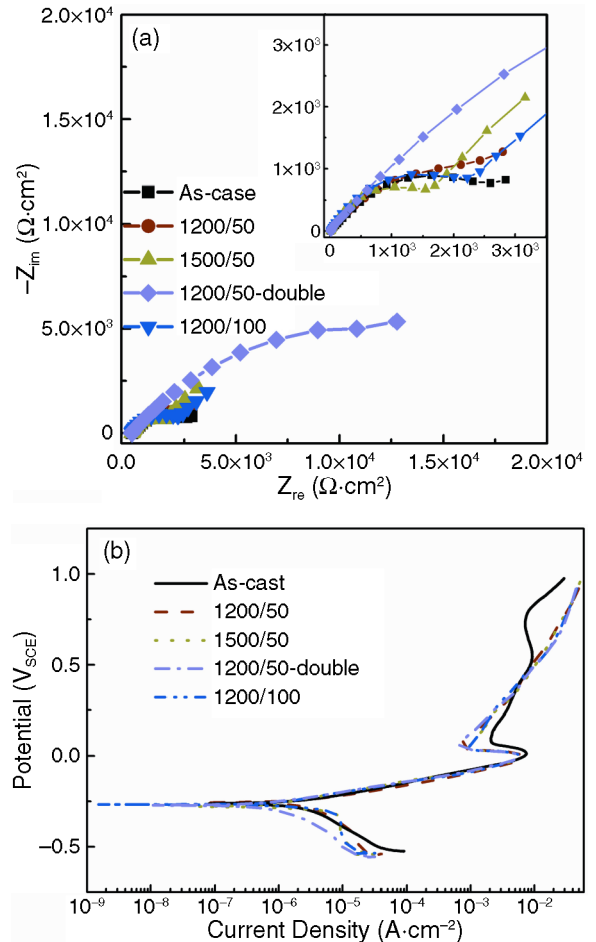


FIGURE 3. (a) Nyquist plots and (b) polarization curves of as-cast and processed NAB with different parameters.

introduced more severe plastic deformation. Therefore, relatively high residual stress might be left in the sample during the cooling process. Residual stress caused by FSP was reported to make the material less resistant to corrosion. Lynch, et al., pointed out that the friction stir processed Mn-Cu alloy without residual stress relieving suffered similar dealloying depth as the as-cast sample, while the processed sample with stress relieving by heat treatment possessed smaller dealloying depth than the as-cast one.³³ Therefore, the growth of the recrystallized grains and higher residual stress decreased the corrosion resistance.

With increasing the traverse speed, more β' , which was detrimental for the corrosion resistance,³⁴ formed in the SZ instead of α and κ phases due to the higher cooling rate. It was also reported in the FSW of dual-phase brass (Cu-38Zn Cu alloy) plates that β' , which had poor deformation ability and high hardness, inhibited the dynamic recrystallization of grains.³⁵ As a result of the increase of β' in the present study, the number of non-recrystallized grains increased. The residual stress also might be higher compared with that for the processed NAB with lower

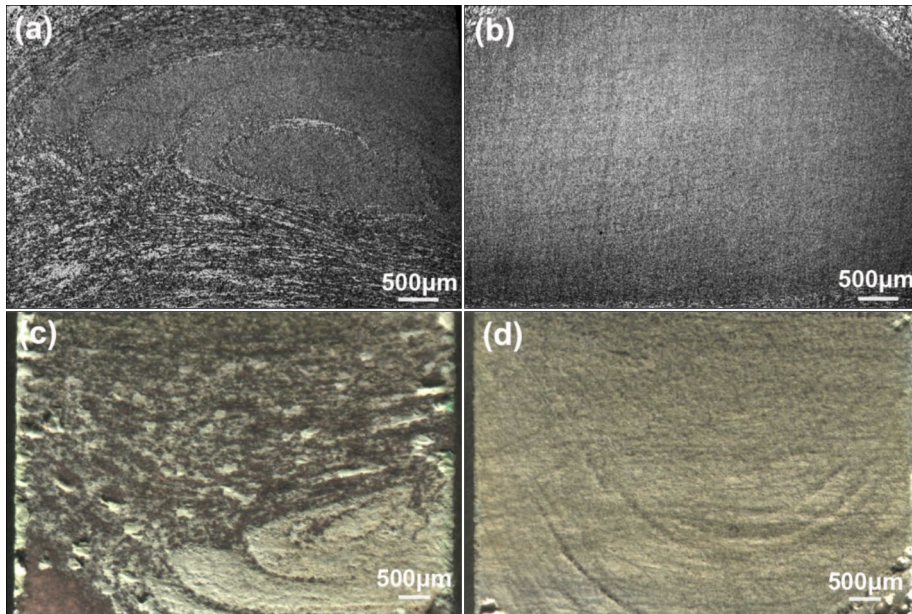


FIGURE 4. Surface morphologies of SZ before and after polarization for (a, c) 1500/50 and (b, d) 1200/50-double.

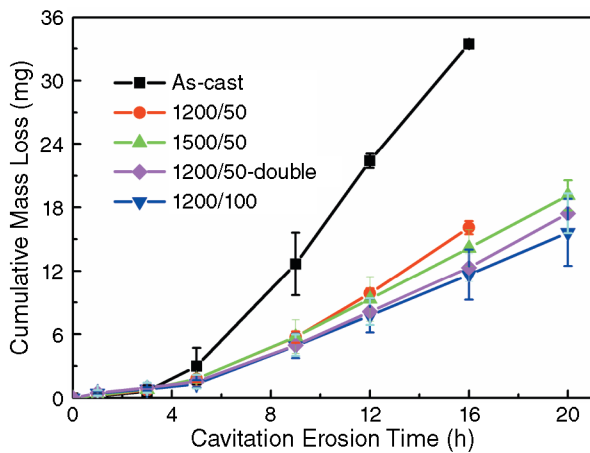


FIGURE 5. Cumulative mass losses as a function of cavitation erosion time for processed NAB with different parameters.

traverse speed. It was reported that the peak longitudinal stresses increased with increasing the traverse speed in aluminum alloy (AA)5083 (UNS A95083) friction stir welds, probably because of the steeper thermal gradients during welding and the reduced time for stress relaxation to occur.³⁶ Besides the above factors, the onion ring pattern in the SZ, which indicated the microstructure heterogeneity, was more apparent at high traverse speeds.⁶ The more heterogeneous microstructure could also cause the inferior corrosion resistance of 1200/100.

For 1200/50-double, the two-pass FSP further homogenized the microstructure and reduced the number of non-recrystallized grains compared with the one-pass FSP. Furthermore, the second pass also acted as a heat treatment for the first-pass FSP and

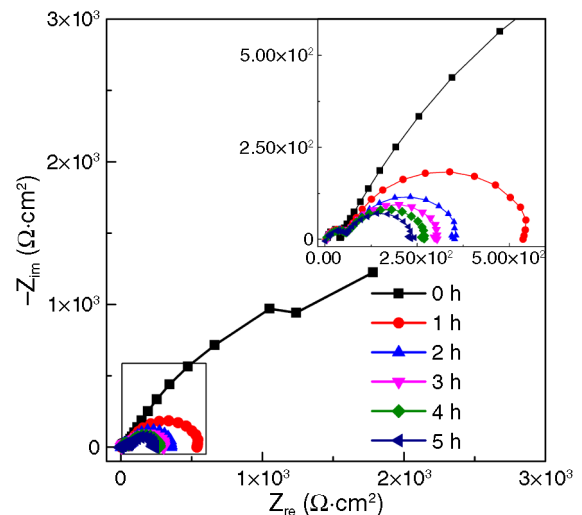


FIGURE 6. Nyquist plots of 1200/100 after different cavitation erosion time.

therefore released the residual stress. It was reported that the residual stress declined with increasing the number of friction stir welding passes for AA7050-T7451 (UNS A97050-T7).³⁷ Therefore, 1200/50-double exhibited the highest corrosion resistance.

Except for 1200/50-double, the processed NAB exhibited severe localized corrosion after polarization in Figure 4. The non-uniform corrosion was caused by the microstructure heterogeneity. β' was anodic compared to α , so the material underwent preferential dissolution and pits formed there. For the Widmanstätten, banded, and stream-like microstructures, α and β' were unevenly distributed and β' were concentrated at some areas, as shown in Figure 2; therefore, it was

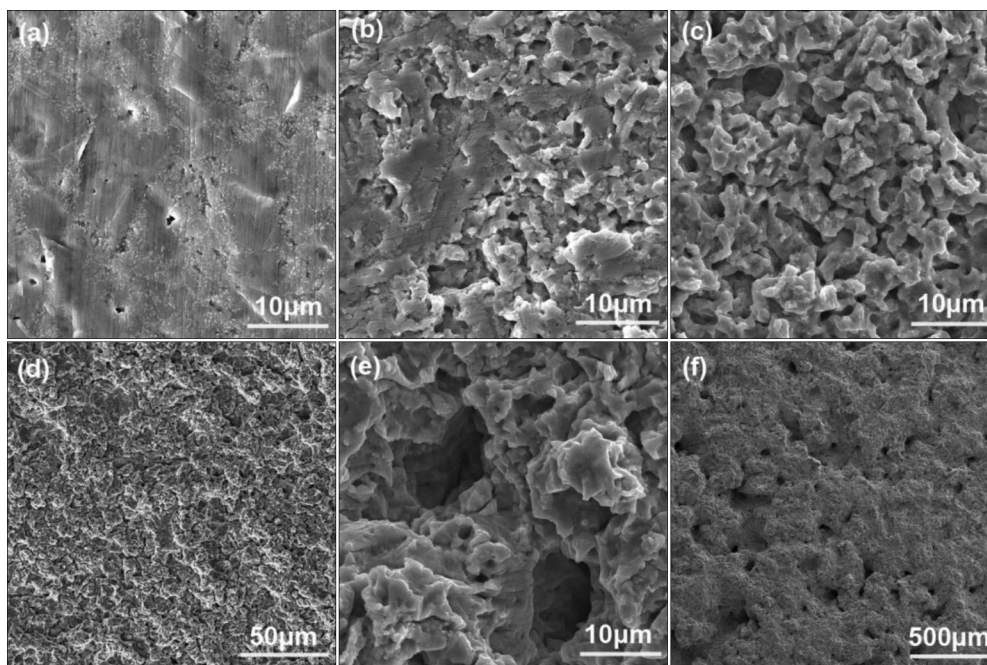


FIGURE 7. Damaged surface morphologies after cavitation erosion for different times. 1200/100: (a) 1 h, (b) 3 h, (c) 5 h, (d) 20 h; as-cast NAB: (e) 5 h, and (f) 16 h.

easy for the growth of pits. For the equiaxed microstructure, the even distribution of α and β' inside contributed to the highest localized corrosion resistance. For 1200/50-double, the surface was uniformly corroded after polarization since it possessed the largest area of equiaxed microstructure.

Cavitation Erosion Behavior — Since FSP refined and homogenized the cast microstructure, and eliminated the casting porosities, the mechanical properties of as-cast NAB were greatly improved. Therefore, the cavitation erosion resistance was much higher for the processed NAB compared with the as-cast one, as shown in Figure 5. However, the processed NAB exhibited similar cavitation erosion behaviors. According to Oh-ishi's and McNelley's studies, when the rotating rate exceeded 800 rpm, the surface temperature was estimated to be about 1,030°C, and the 1/3 depth location was about 930°C.⁸ So, in the top surface, the material was fully transformed to single β phase, and Widmanstätten α and β' formed during the following fast cooling process. In the Subsurface, due to the relatively lower temperature, partial α transformed to β and banded α and β' formed during the cooling process.

The top surface with Widmanstätten structure was quite thin according to the metallographic observation and was easily removed by grinding during the sample preparation. Therefore, for all of the samples with different processing parameters, it was the Subsurface, namely, the same microstructure, that was exposed to cavitation erosion. This might be the reason for the similar cavitation erosion behaviors of the NAB with different processing parameters. Further-

more, the cavitation erosion intensity selected in the present study might be so strong that it failed to distinguish the difference among the processed NAB with different processing parameters. Therefore, similar studies should be done with smaller cavitation erosion intensity in the future, i.e., with a vibrating amplitude less than 60 μm .

Although the results overlapped with each other, 1200/100 exhibited the highest cavitation erosion resistance, followed by 1200/50-double and 1500/50, and 1200/50 was the least cavitation-erosion-resistant. In our previous study concerning the effect of processing parameters on mechanical properties of NAB, the results showed that compared with 1200/50, the ultimate tensile strength decreased slightly with the increase of rotating rate or traverse speed, and the elongation of the sample subjected to two-pass FSP was much higher than the single-pass processed ones.⁶ The cavitation erosion results were not wholly consistent with the reported mechanical properties results since the whole SZ was evaluated there, while only the Subsurface of the SZ was evaluated in the present study.

Compared with 1200/50, the heat input of 1500/50 was larger, so at the Subsurface more primary α with lower hardness transformed to β and the retained α experienced sufficient recrystallization. Therefore, in the cooling process, more β' with higher hardness and refined α formed; correspondingly, the hardness was higher for the Subsurface of 1500/50. Since cavitation erosion resistance was positively correlated with hardness, the mass loss of 1500/50

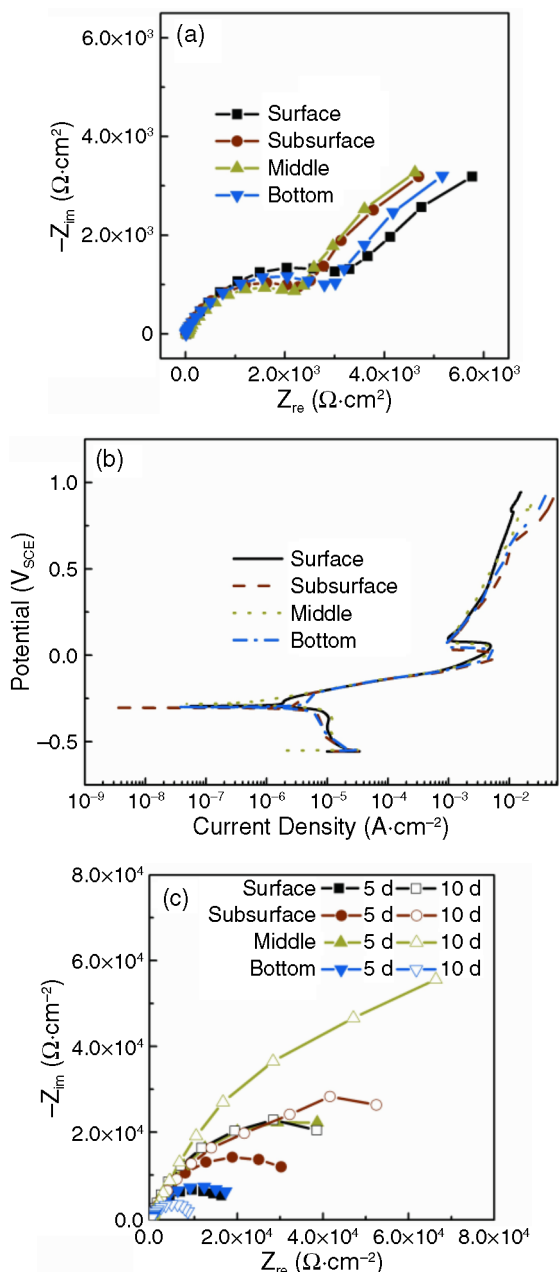


FIGURE 8. (a) Initial Nyquist plots, (b) polarization curves, and (c) Nyquist plots after different immersion times for samples in SZ along the plate thickness.

was smaller. 1200/50-double exhibited much higher elongation and further homogenized microstructure. After the first FSP pass, there were still some primary α grains, which were incompletely recrystallized. The second FSP pass reduced the number of incompletely recrystallized α grains and further refined them. The improved ductility and refined microstructure were preferable to resist cavitation erosion. For 1200/100, due to the fast traverse speed, there was no abundant time for the phase transformation, so less κ phases were dissolved and the retained κ phases, which were broken up due to the severe plastic deformation, acted

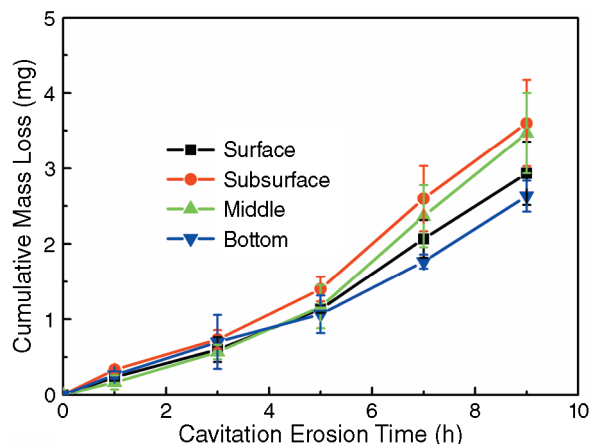


FIGURE 9. Cumulative mass losses as a function of cavitation erosion time for samples in SZ along the plate thickness.

as strengthening phases. Because of the fast cooling rate, the growth of recrystallized α grains was suppressed, so 1200/100 possessed the highest cavitation erosion resistance.

Under continuous cavitation erosion, the surface became rougher due to the deformation as well as the growth of cracks and cavities. All of these made the surface more active and less corrosion-resistant. As shown in Figure 6, the corrosion resistance for the processed NAB decreased by increasing the cavitation erosion time. At the initial period of cavitation erosion, the processed NAB exhibited plastic deformation for its good ductility, and extrusion were seen in Figure 7(a). With increasing the cavitation erosion time, cavities formed on the surface (Figures 7(b) and [c]). Correspondingly, inductive resistive behavior was shown at the lower frequency in the Nyquist plot in Figure 6 and obvious mass loss was found in Figure 5. In comparison, large cavities and long cracks on the surface of the as-cast NAB caused remarkable mass loss, as shown in Figures 7(e) and (f).

The tensile properties including yield strength (YS), ultimate tensile strength (UTS), and elongation (EL) of the processed and as-cast NAB are listed in Table 2.⁶ As a result of the improved ductility, the processed NAB exhibited more plastic behavior, and the extending of cavities and cracks along the depth to the substrate with increasing the cavitation erosion time was effectively hindered, so the cavitation erosion damage was greatly reduced by FSP.

Corrosion and Cavitation Erosion Behaviors for Samples in the Stirred Zone Along the Plate Thickness

Corrosion Behavior — The initial Nyquist plots and polarization curves were similar for the four positions in the SZ of the processed NAB, as shown in Figures 8(a) and (b). Therefore, the heterogeneous microstructure in the SZ would not introduce severe

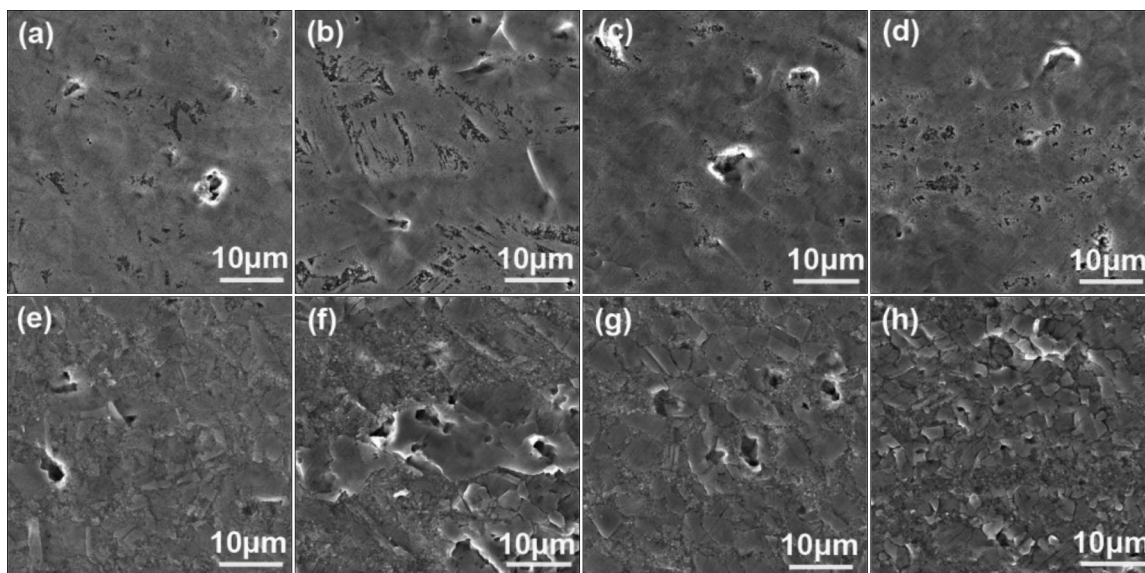


FIGURE 10. Damaged surface morphologies for samples in SZ along the plate thickness after cavitation erosion for different times. Surface: (a) 1 h, (e) 3 h; Subsurface: (b) 1 h, (f) 3 h; Middle: (c) 1 h, (g) 3 h; and Bottom: (d) 1 h, (h) 3 h.

TABLE 2

Tensile Properties of As-Cast and Processed Ni-Al Bronze^(A)

Sample	Direction ^(B)	YS (MPa)	UTS (MPa)	EL (%)
FSP samples	Traverse/longitudinal	436 to 502/415 to 479	790 to 852/776 to 837	20 to 29/25 to 31
As-cast	—	282±2	645±29	18±6.6

^(A) Data from Ref. 6.

^(B) Traverse and longitudinal correspond to directions perpendicular and parallel to the processing direction of FSP, respectively.

galvanic corrosion. Film formed for all the four positions after immersion in 3.5 wt% NaCl solution, as shown in Figure 8(c), since the electrochemical impedance after 10 days' immersion increased compared to the initial impedance. Except for the Bottom (to be studied in the future), the electrochemical impedance increased with the immersion time and this indicated continuous film growth. The film on the Middle was the most protective since its electrochemical impedance was the largest. For the Middle sample with equiaxed structure, α and β' were distributed evenly, while it was not the case for the other three positions. Since films formed over different phases might be different in component, structure, and growth rate, cracks would form in the film as a result of the growth stress if the microstructure was heterogeneous. The evenly distributed microstructure attributed to a homogeneous film, so the film on the Middle was of the highest impedance.

Cavitation Erosion Behavior — The results of cavitation erosion tests showed that the Bottom sample was the most cavitation-erosion-resistant, followed by the Surface, Middle, and Subsurface. The vertical hardness profiles through the center of the SZ in our previous research suggested that the top and bottom of the SZ had higher hardness than the cen-

ter.⁶ The grains in the Bottom were the finest in the SZ, as shown in Figure 2; therefore, the Bottom had the highest hardness according to the Hall-Petch relationship. Mahoney, et al., also reported that the Widmanstätten structure (corresponding to the Surface) in the SZ possessed higher tensile strength than the equiaxed and lamellar structures (corresponding to the Middle and Subsurface samples).³⁸ Therefore, the Surface was more cavitation-erosion-resistant than the Middle and Subsurface. Evidence could also be seen from the damaged morphologies shown in Figure 10. For the four positions where four positions were found in α phase at the initial period of cavitation erosion, since α had a face-centered cubic (fcc) structure³⁹ and it experienced plastic deformation under the cavitation stress. β' phase was preferentially corroded since it was anodic compared to α phase, so the surface at β' phase was relatively rough. With increasing the cavitation erosion time, large cavities appeared inside α phase, as shown in the banded and equiaxed microstructures in Figures 10(f) and (g), since the continuous cavitation stress caused the fatigue failure of α phase. The Widmanstätten and stream-like structures suffered less damage, as shown in Figures 10(e) and (h), since the former mainly experienced deformation rather than the fatigue failure under cavitation stress

due to the higher tensile strength. However, the error bars of the results for the four samples overlapped with each other, possibly due to the short cavitation erosion period, i.e., 9 h in the present study.

The cavitation erosion and corrosion results of the four different microstructures in the SZ through FSP could be guides for other processing methods, such as heat treatment and some plastic processing methods, to get the right microstructure of NAB suitable for the real service environment.

CONCLUSIONS

- ❖ The SZ of the processed NAB with different FSP parameters were characterized by Widmanstätten, banded, equiaxed, and stream-like microstructures from the surface to the bottom along the plate thickness, while 1200/50-double possessed equiaxed microstructure in most of its SZ.
- ❖ 1200/50-double possessed the best corrosion resistance since it had the most homogeneous microstructure.
- ❖ All of the processed NAB exhibited greatly improved cavitation erosion resistance compared with the as-cast one. 1200/100 showed slightly higher cavitation erosion resistance than other processed NAB for its finest microstructure due to the fastest cooling rate during FSP. 1200/50-double rated second for its highly improved ductility and further refined microstructure.
- ❖ Four positions of the SZ in 1200/50 along the plate thickness differed little in the initial impedance and polarization curves, while after 10 days' immersion in 3.5 wt% NaCl solution, the Middle exhibited the highest impedance since the evenly distributed equiaxed α and β' phases contributed to a more homogeneous film.
- ❖ Among the four positions in the SZ, the Bottom was the most cavitation erosion resistant since it had the finest grain size.

ACKNOWLEDGMENTS

This work was supported by the National Natural Science Foundation of China (no. 51131008).

REFERENCES

1. R.S. Mishra, Z.Y. Ma, *Mater. Sci. Eng. R* 50 (2005): p. 1.
2. W.M. Thomas, E.D. Nicholas, J.C. Needham, M.G. Murch, P. Temple-Smith, C.J. Dawes, "Friction Stir Butt Welding," G.B. Patent Application no. 9125978.8, 1991.

3. S. Jana, R.S. Mishra, J.B. Baumann, G. Grant, *Acta Mater.* 58 (2010): p. 989.
4. M.L. Santella, T. Engstrom, D. Storjohann, T.Y. Pan, *Scr. Mater.* 53 (2005): p. 201.
5. K. Surekha, B.S. Murty, K. Prasad Rao, *Solid State Sci.* 11 (2009): p. 907.
6. D.R. Ni, P. Xue, D. Wang, B.L. Xiao, Z.Y. Ma, *Mater. Sci. Eng. A* 524 (2009): p. 119.
7. D.R. Ni, B.L. Xiao, Z.Y. Ma, Y.X. Qiao, Y.G. Zheng, *Corros. Sci.* 52 (2010): p. 1610.
8. K. Oh-ishi, T.R. McNelley, *Metall. Mater. Trans. A* 35A (2004): p. 2951.
9. M. Atapour, A. Pilchak, G.S. Frankel, J.C. Williams, *Corros. Sci.* 52 (2010): p. 3062.
10. W. Woo, H. Choo, M.B. Prime, Z. Feng, B. Clausen, *Acta Mater.* 56 (2008): p. 1701.
11. Z. Yu, H. Choo, Z. Feng, S.C. Vogel, *Scr. Mater.* 63 (2010): p. 1112.
12. H.S. Grewal, H.S. Arora, H. Singh, A. Agrawal, *Appl. Surf. Sci.* 268 (2013): p. 547.
13. J.D. Escobar, E. Velásquez, T.F.A. Santos, A.J. Ramirez, D. López, *Wear* 297 (2013): p. 998.
14. K. Oh-ishi, T.R. McNelley, *Metall. Mater. Trans. A* 36A (2005): p. 1575.
15. J. Gandra, R.M. Miranda, P. Vilaca, *Mater. Sci. Eng. A* 528 (2011): p. 5592.
16. K. Elangovan, V. Balasubramanian, *Mater. Des.* 29 (2008): p. 362.
17. W.F. Xu, J.H. Liu, H.Q. Zhu, *Electrochim. Acta* 55 (2010): p. 2918.
18. E.A. Culpan, G. Rose, *Br. Corros. J.* 14 (1979): p. 160.
19. A. Al-Hashem, P.G. Caceres, W.T. Riad, H.M. Shalaby, *Corrosion* 51 (1995): p. 331.
20. A. Karimi, J.L. Martin, *Int. Metals Rev.* 31 (1986): p. 1.
21. R.H. Richman, W.P. McNaughton, *Wear* 140 (1990): p. 63.
22. W. Będkowski, G. Gasiak, C. Lachowicz, A. Lichtarowicz, T. Łagoda, E. Macha, *Wear* 230 (1999): p. 201.
23. E.A. Culpan, G. Rose, *J. Mater. Sci.* 13 (1978): p. 1647.
24. A. Jahanafrooz, F. Hasan, G.W. Lorimer, N. Ridley, *Metall. Trans. A* 14A (1983): p. 1951.
25. C.H. Tang, F.T. Cheng, H.C. Man, *Mater. Sci. Eng. A* 373 (2004): p. 195.
26. C.H. Tang, F.T. Cheng, H.C. Man, *Surf. Coat. Technol.* 200 (2006): p. 2602.
27. S. Hanke, A. Fischer, M. Beyer, J. Santos, *Wear* 273 (2011): p. 32.
28. K.S. Park, S. Kim, *J. Electrochem. Soc.* 158 (2011): p. C335.
29. W.A. Palko, R.S. Fielder, P.F. Young, *Mater. Sci. Forum* 426-432 (2003): p. 2909.
30. Y.G. Zheng, Q.N. Song, S.L. Jiang, D.R. Ni, Z.Y. Ma, "Comparison of Corrosion and Cavitation Erosion Behaviors Between the As-Cast and Friction-Stir Processed Nickel Aluminum Bronze," CORROSION 2013, paper no. 0002322 (Houston, TX: NACE International, 2013).
31. ASTM International G32-03, "Standard Test for Cavitation Erosion Using Vibratory Apparatus" (West Conshohocken, PA: ASTM International, 2003).
32. J.R. Scully, D.C. Silverman, M.W. Kendig, eds., *Electrochemical Impedance: Analysis and Interpretation* (West Conshohocken, PA: ASTM International, 1993), p. 1.
33. S.P. Lynch, D.P. Edwards, A. Majumdar, S. Moutsos, M.W. Mahoney, *Mater. Sci. Forum* 426-4 (2003): p. 2903.
34. P. Weill-Couly, D. Arnaud, *Fonderie* 28 (1973): p. 123.
35. G.M. Xie, Z.Y. Ma, L. Geng, *Philos. Mag.* 89 (2009): p. 1505.
36. M. Peel, A. Steuwer, M. Preuss, P.J. Withers, *Acta Mater.* 51 (2003): p. 4791.
37. R. Brown, W. Tang, A.P. Reynolds, *Mater. Sci. Eng. A* 513-514 (2009): p. 115.
38. M.W. Mahoney, W.H. Bingel, S.R. Sharma, R.S. Mishra, *Mater. Sci. Forum* 426-432 (2003): p. 2843.
39. F. Hasan, A. Jahanafrooz, G.W. Lorimer, N. Ridley, *Metall. Trans. A* 13A (1982): p. 1337.